

Supporting Information: Systematic Study of Nanocrystal Clusters Assembled by Solvent Evaporation

Elizabeth Macias, Tommy Waltmann, and Alex Travasset*

*Department of Physics & Astronomy and Ames Laboratory - USDOE, Iowa State
University, Ames, IA 50011, USA*

E-mail: trvsst@ameslab.gov

Pressure in different solvents

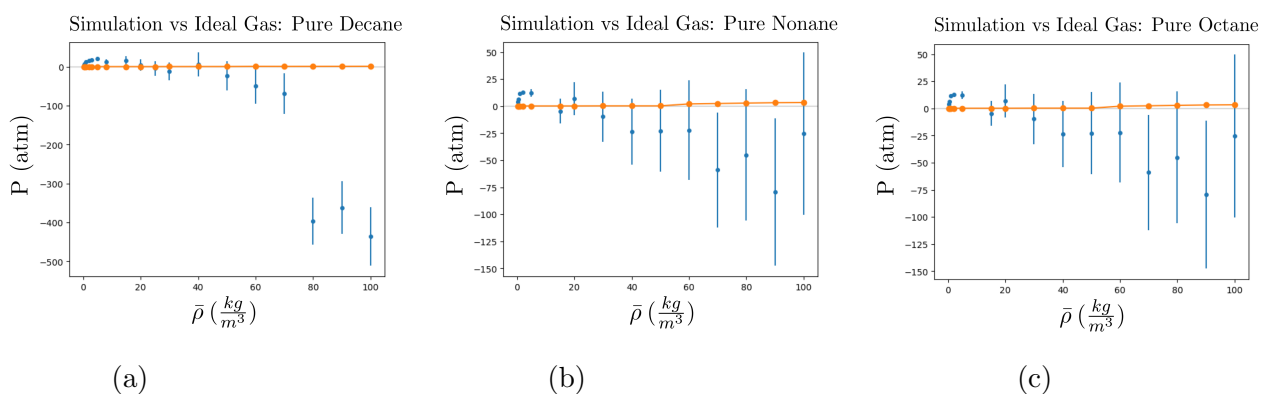


Figure S1: Simulated pressure, in blue, plotted against the calculated pressure Eq. 4, in orange for (a) Decane, (b) Nonane, and (c) Octane.

Pressure as a Function of Average Density

Fig. S2 shows pressure vs $\bar{\rho}$, for Decane, Nonane, and Octane. For Decane, we note that the pressure is negative for densities approximately below $700 \frac{kg}{m^3}$ and positive above.

$$P - P_{ref} = \frac{1}{k_T} \ln\left(\frac{\rho}{\rho_{ref}}\right) \quad (S1)$$

where P_{ref} and ρ_{ref} are reference points from the plot and k_T is the isothermal compressibility. This equation is derived from the following thermodynamic relationship,

$$\frac{\partial P}{\partial \rho}^{T,N} = \frac{1}{k_T \rho} \quad (S2)$$

for a single phase system where the number of particles and the temperature is fixed we estimate the isothermal compressibility. From the fit, we see that $k_T = 8.66 \times 10^{-05} atm^{-1}$, $k_T = 8.06 \times 10^{-05} atm^{-1}$, $k_T = 7.34 \times 10^{-05} atm^{-1}$ and for Decane, Nonane, and Octane respectively. There are large errors in the pressure calculation, since fluctuations in pressure are related to fluctuations in temperature according to

$$\Delta P = \frac{\beta}{k_T} \Delta T \quad (S3)$$

where β is the Boltzmann constant. Fig. S2 shows $\frac{\Delta P}{\Delta T}$ versus average density for Decane, Nonane and Octane. Therefore, We see that we have fluctuations of around $10 \frac{bar}{K}$ for the lower end of the density range. The maroon vertical line corresponds to the experimental liquid density while the orange line corresponds to the density, at which the solvent appears to be pure liquid.

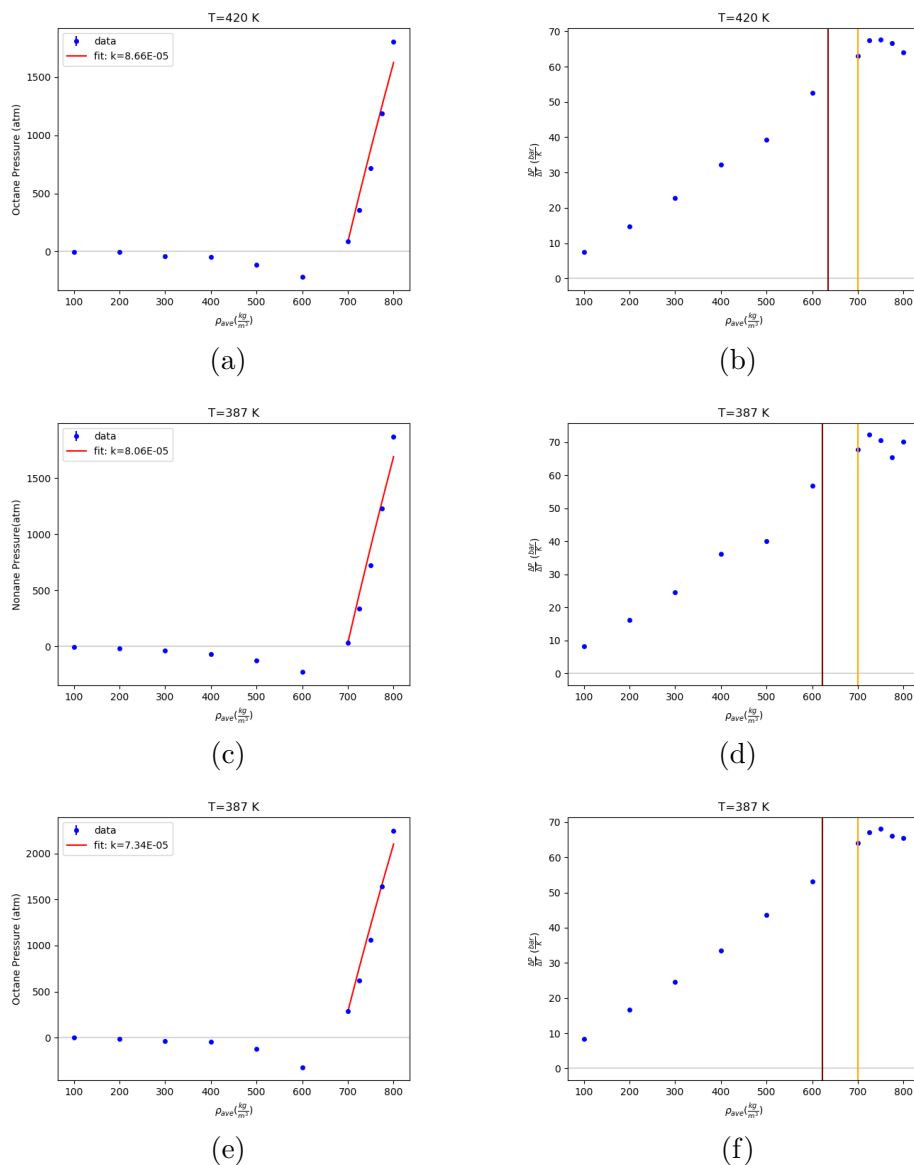


Figure S2: Left: The pressure for pure (a) Decane, (c) Nonane, and (e) Octane. The compressibility is $k_T = 8.66 \times 10^{-05} atm^{-1}$, $k_T = 8.06 \times 10^{-05} atm^{-1}$, and $k_T = 7.34 \times 10^{-05} atm^{-1}$ for Decane, Nonane, and Octane respectively. Right: Fluctuation in pressure for (b) Decane, (d) Nonane, and (f) Octane. The maroon vertical line corresponds to the experimental liquid density while the orange line corresponds to the density, from Fig. S3, at which the solvent appears to be pure liquid.

Phase coexistence as a function of average densities

Fig. S3 shows the particle distributions vs average densities. We see that as we increase the average density, we go from having two peaks in our distribution to one peak. For the case where the system has two peaks, we can interpret the lower and higher density peaks as those which correspond to the gas and liquid particles, respectively. As for the single-peak case, we can interpret that as due to a system with only liquid particles. Thus, we interpret the transition from two to one peaks as the system transitioning from liquid-gas coexistence to a liquid phase.

Moreover, we plot the gray and maroon vertical lines that correspond to the experimental saturation liquid and vapor particle densities, respectively, and we see that the lines match with the distribution peaks. This further reassures our interpretation. The Decane saturated liquid and vapor densities for 420 K were taken from ref¹ while the Nonane and Octane saturated liquid and vapor densities at 387 K were extrapolated from data provided in ref². The referenced Octane and Nonane data is presented in tables S1 and S2 respectively.

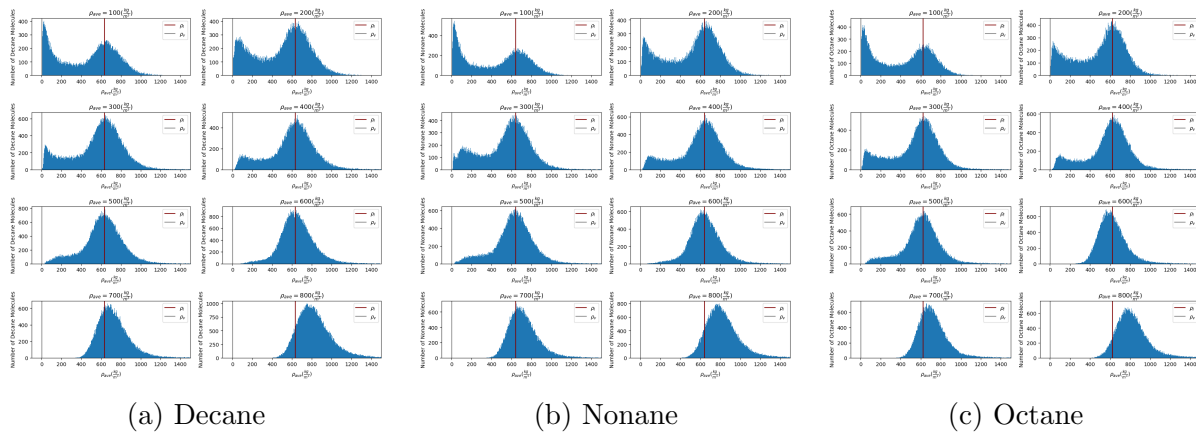


Figure S3: Density distribution functions of (a) Decane (b) Nonane and (c) Octane for different average densities. For each average density, we ran the simulation for 1E6 time steps and distributed the data over 99 time frames. Therefore, we constructed the density distribution by accumulating the particle data from all 999 frames. The gray and maroon vertical lines correspond to the experimental saturation liquid and vapor particle densities, respectively. The experimental values for saturation liquid and vapor densities are, Decane: $\rho_l = 635.0 \frac{kg}{m^3}$ and $\rho_v = 2.816 \frac{kg}{m^3}$; Nonane: $\rho_l = 641.058 \frac{kg}{m^3}$ and $\rho_v = 1.3875 \frac{kg}{m^3}$; Octane: $\rho_l = 622.151 \frac{kg}{m^3}$ and $\rho_v = 2.70495 \frac{kg}{m^3}$.

Table S1: Pure Nonane saturated liquid(vapor)densities, $\rho_l(\rho_g)$, for different values of temperature. This data was used to extrapolate the saturated liquid and vapor densities at 387 K and was derived from ref². The density was converted from $\frac{ml}{mol}$ to $\frac{kg}{m^3}$.

	Temperature/K				
	361	367	373	378	384
$\rho_l/\frac{kg}{m^3}$	663.12	658.08 ₅	653.02 ₅	648.76	643.65
$\rho_g/\frac{kg}{m^3}$	0.5744 ₈	0.7131 ₉	0.8778	1.0373	1.2586 ₅
	Temperature/K				
	390	396	401	407	
$\rho_l/\frac{kg}{m^3}$	638.46	633.22 ₉	628.82	623.50	
$\rho_g/\frac{kg}{m^3}$	1.5163	1.8146	2.0974	2.4821	

Table S2: Pure Octane saturated liquid(vapor)densities, $\rho_l(\rho_g)$, for different values of temperature. This data was used to extrapolate the saturated liquid and vapor densities at 387 K and was derived from ref². The density was converted from $\frac{ml}{mol}$ to $\frac{kg}{m^3}$.

	Temperature/K				
	360	368	376	384	392
$\rho_l/\frac{kg}{m^3}$	646.37 ₇	639.32	632.17 ₅	624.91	617.54 ₇
$\rho_g/\frac{kg}{m^3}$	1.1711	1.5214	1.9505 ₇	2.4708	3.0950
	Temperature/K				
	400	408			
$\rho_l/\frac{kg}{m^3}$	610.02 ₈	602.40			
$\rho_g/\frac{kg}{m^3}$	3.8377 ₈	4.7147			

Supplementary Results for Different Radius

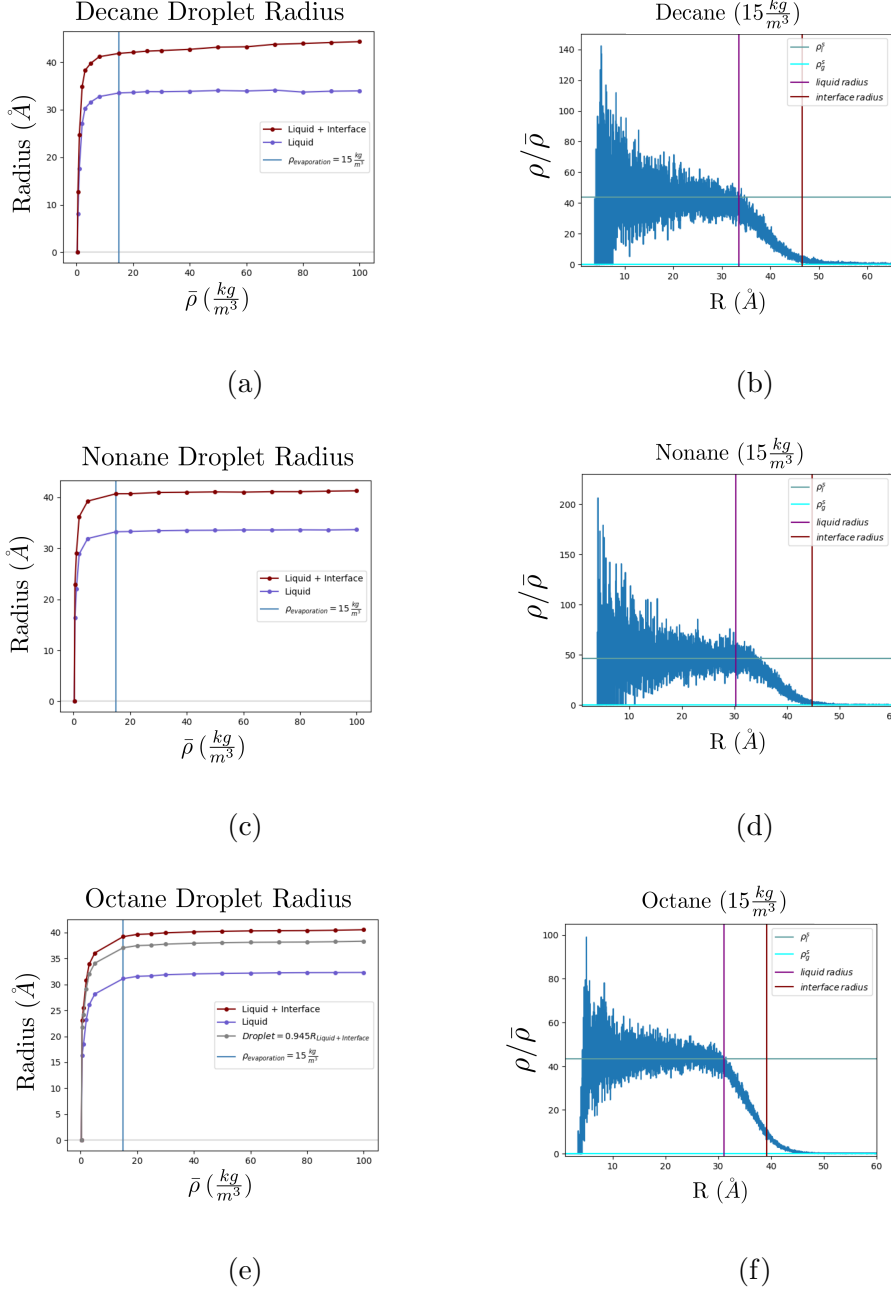


Figure S4: To the left: The droplet radius is in grey. That for the liquid-only and liquid + interface are purple and maroon. The blue vertical line corresponds to the density, from the figure to the right, at which we computed the local density distribution. To the right: The local density with respect to the center of a droplet for a system with mean density $15 \frac{kg}{m^3}$. The light-blue and cyan horizontal bars correspond to mean *liquid* and *vapor* densities ($\bar{\rho}_l$ and $\bar{\rho}_g$), respectively. The purple and maroon vertical lines correspond to the liquid and interface droplet radius. Decane: $\bar{\rho}_l = 655.5 \frac{kg}{m^3}$, $\bar{\rho}_g = 1.104 \frac{kg}{m^3}$; Nonane: $\bar{\rho}_l = 697.7 \frac{kg}{m^3}$, $\bar{\rho}_g = 0.491 \frac{kg}{m^3}$; Octane: $\bar{\rho}_l = 649.3 \frac{kg}{m^3}$, $\bar{\rho}_g = 1.971 \frac{kg}{m^3}$.

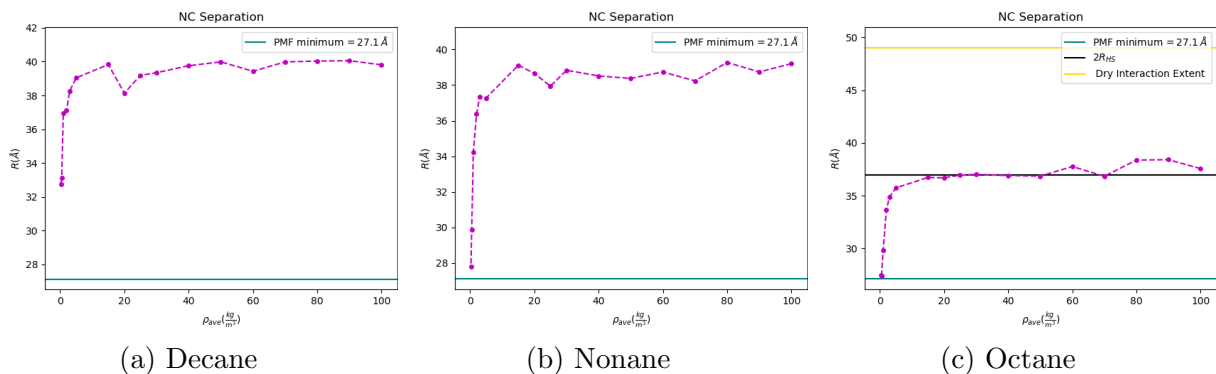


Figure S5: Left: Pair Separation with evaporation. Right: Pair+Solvent droplet radius. The three plots are shown for Decane (top row), Nonane (middle row) and Octane (bottom row).

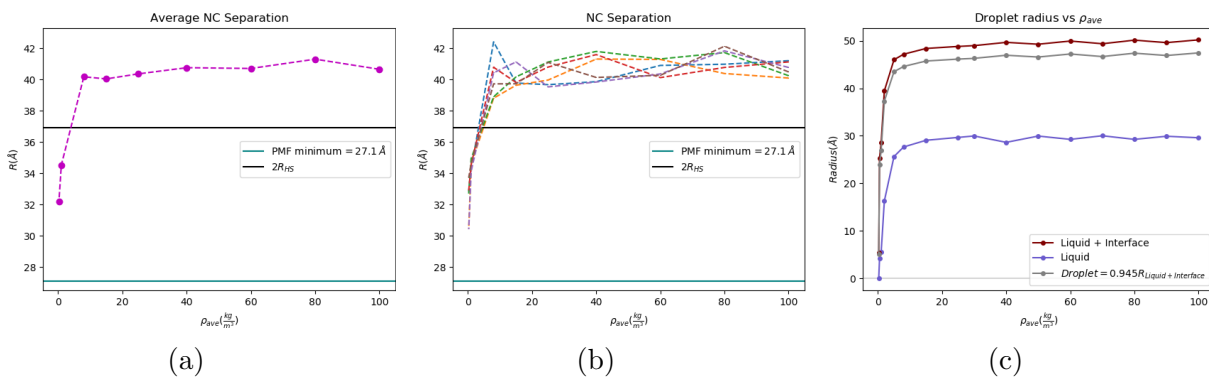


Figure S6: (a).4-*N*+Octane Average Separation with Octane evaporation. (b) 4-*N*+Octane Separation for different NC pairs. (c).4-*N*+Octane droplet radius.

NC Structures

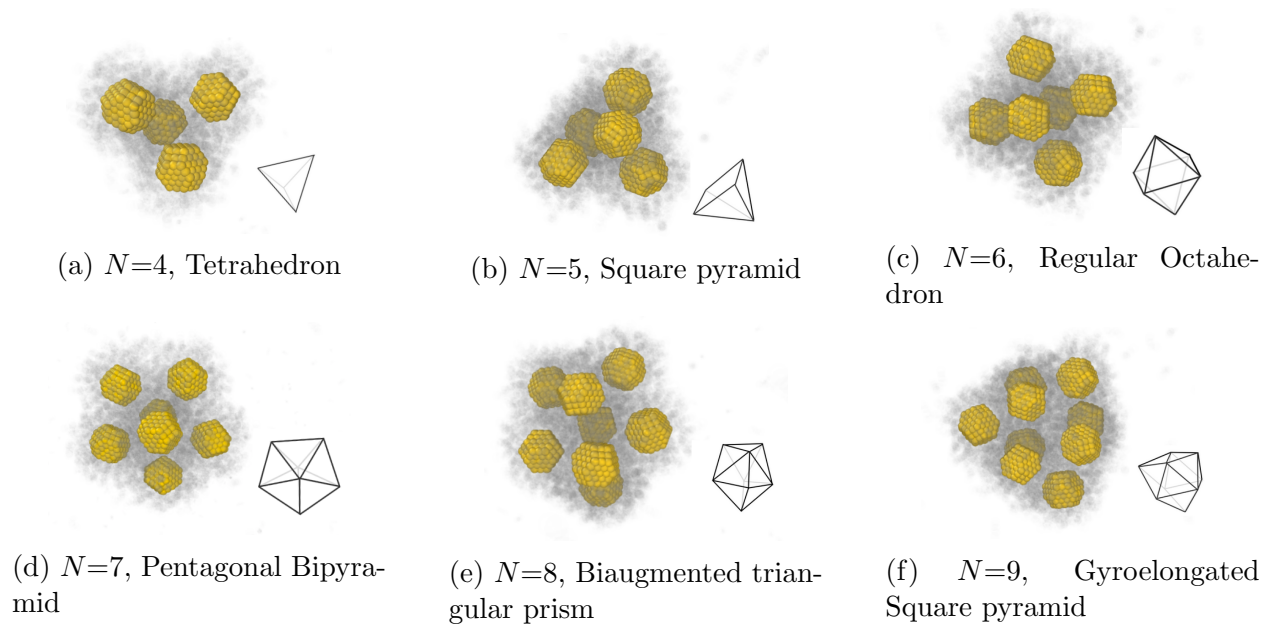


Figure S7: Equilibrium structures: $N=4, 5, 6, 7, 8, 9$.

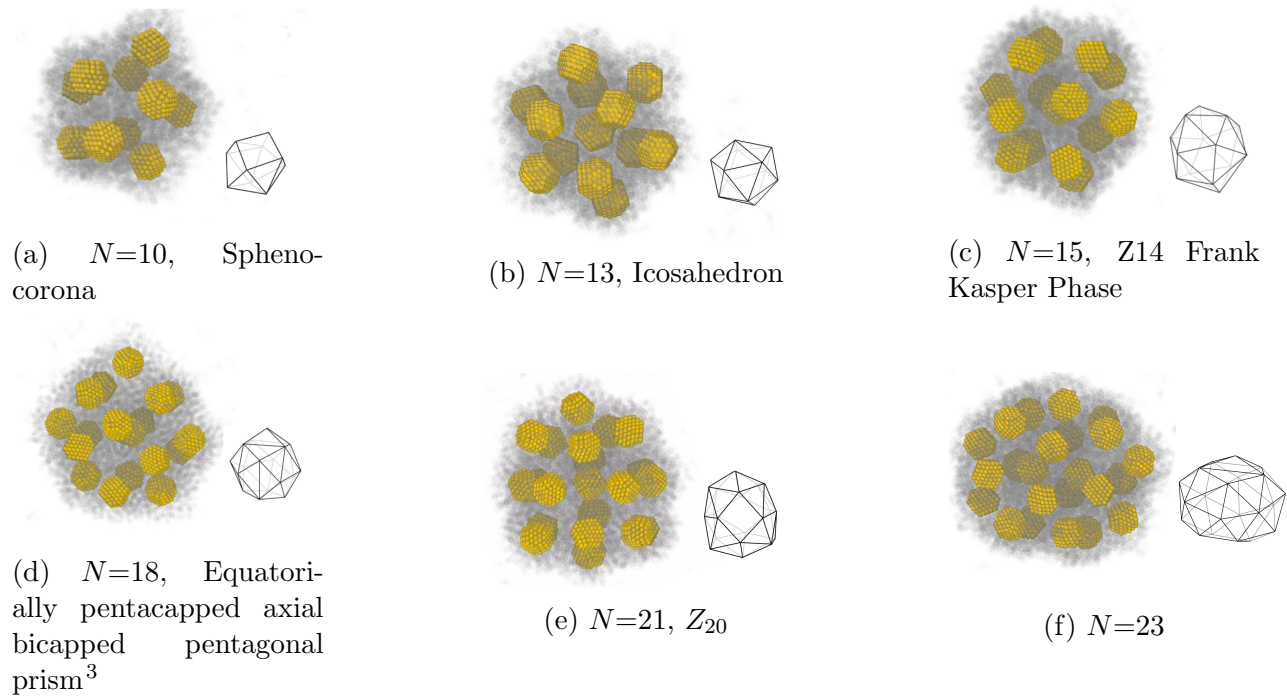


Figure S8: Equilibrium structures: $N=10, 13, 15, 18, 21, 23$.

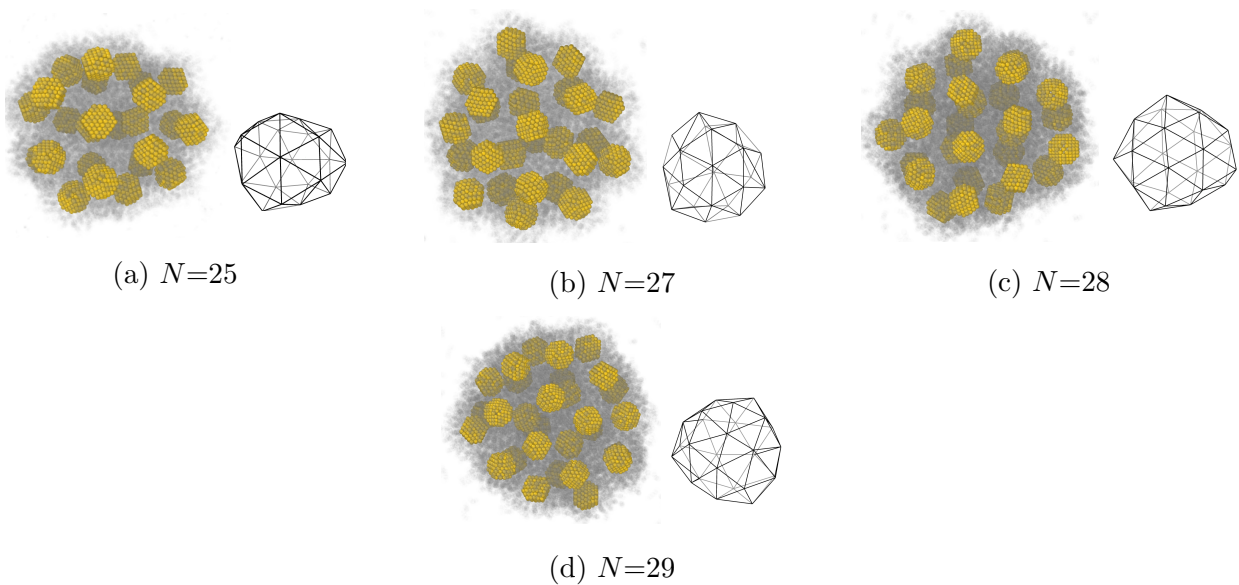
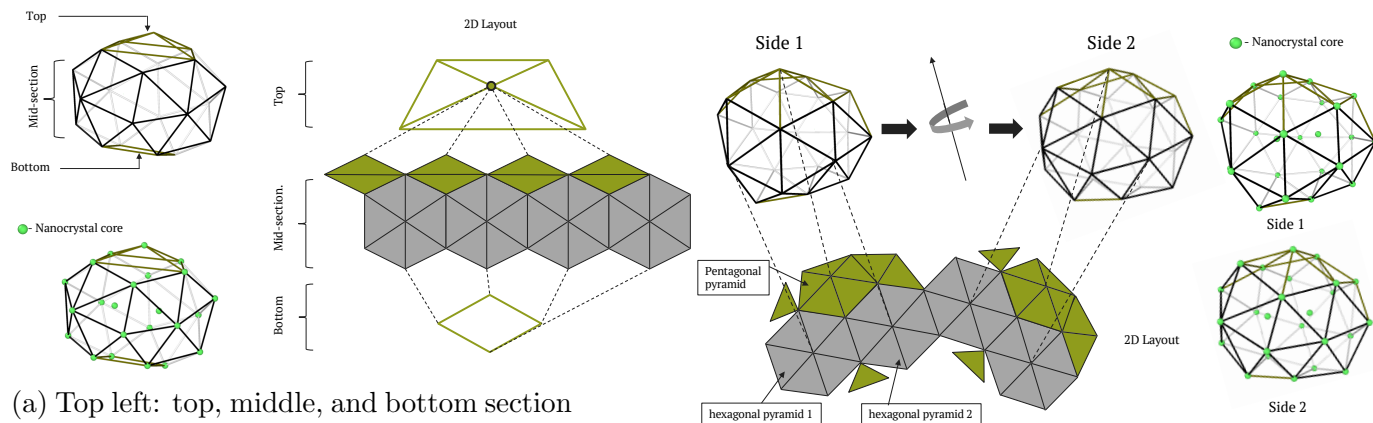
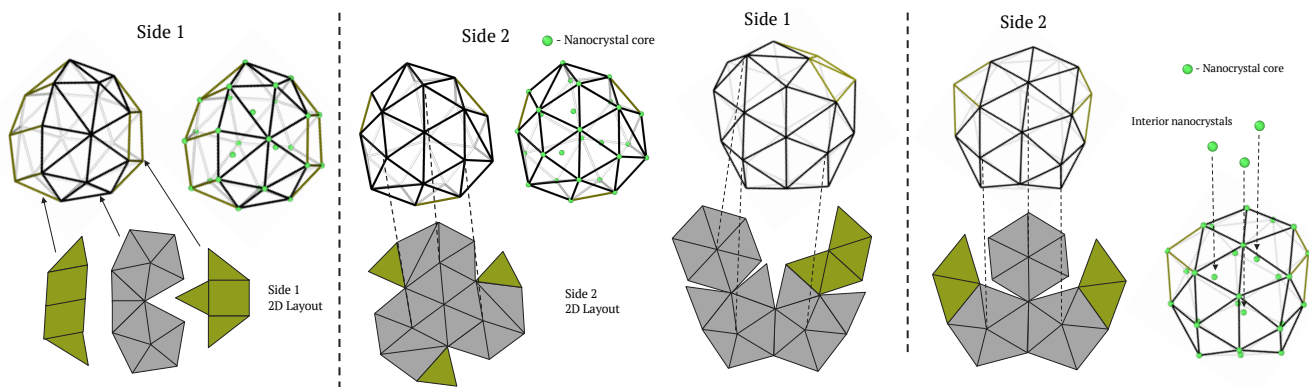


Figure S9: Equilibrium structures: $N=25, 27, 28, 29$.



(a) Top left: top, middle, and bottom section of 3D stick-figure representation of $N=23$ structure. Bottom Left: stick-figure representation with NC cores at their respective vertices. Right: 2D layout of $N=23$ structure.

(b) Structural Analysis for $N=25$. left: Rotation of top left structure, about the axis in the figure, to the side 2. Right: display of NC cores.



(c) Structural Analysis for $N=27$.

(d) Structural Analysis for $N=28$.

Figure S10: Structural Illustration of $N=23$, 25, 27, 28 NC-configurations.

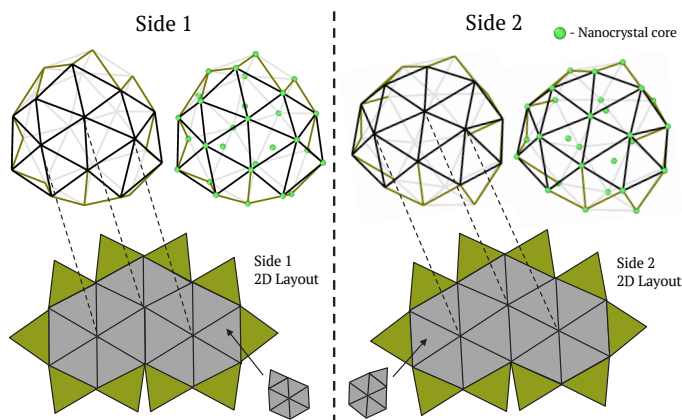


Figure S11: Structural Analysis for $N=29$. The little grey figures indicate what is half the grey area of the larger figures. They indicate half the area since the larger figures are symmetric in their 2D layout.

NC Structures compared to Cambridge database

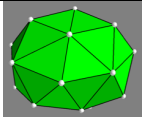
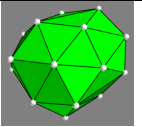
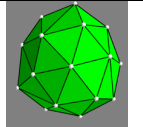
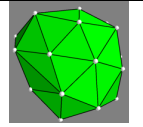
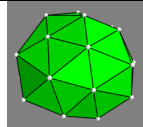
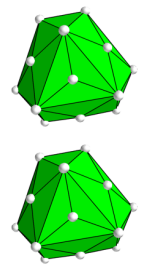
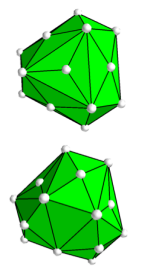
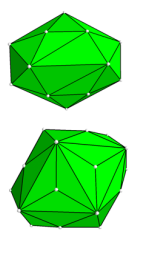
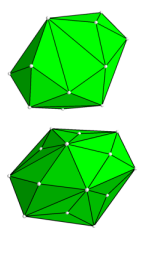
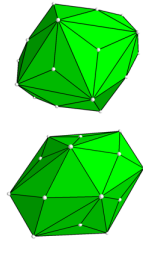
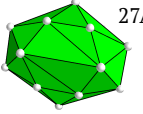
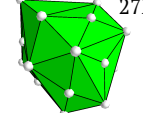

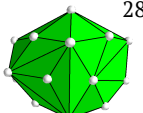
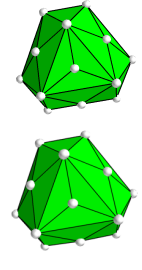
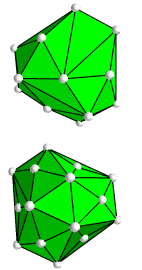
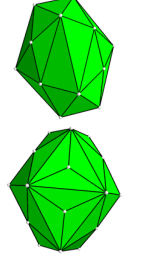
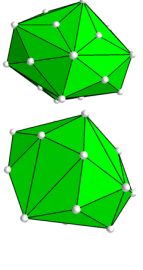
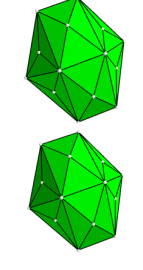
N	23	25	27	28	29
Our Clusters					
Lennard-Jones Cluster					
LJ_13	N/A	N/A	N/A	N/A	N/A
Quantum Lennard-Jones Cluster	N/A	N/A	 	 	N/A
Ar _n for the Aziz Potential					

Figure S12: Comparison of our structures with respect to those in the Cambridge database⁴ for Lennard-Jones potential. The two-image table cells correspond to "back" and "front" images of structures unless otherwise specified. The images were created using the Mayavi python package for all structures in order to create a benchmarked analysis.

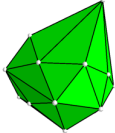
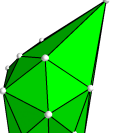
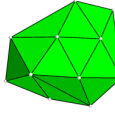
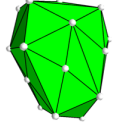
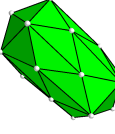
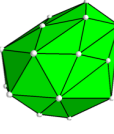
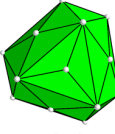
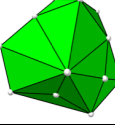
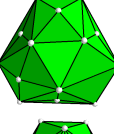
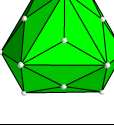
N	23	25	27	28	29
Ar _n ⁺ for a Diatomics-in-Molecules Potential			N/A	N/A	N/A
Ne _n ⁺ Clusters for a Diatomics-in-Molecules Potential			N/A	N/A	N/A
Ar _n Cl ₁₂ for a Diatomics-in-Molecules Potential			N/A	N/A	N/A
Ar _n NO for a Diatomics-in-Molecules Potential	 	 	N/A	N/A	N/A

Figure S13: Comparison of our structures with respect to those in the Cambridge database⁴ for Lennard-Jones potential. The two-image table cells correspond to "back" and "front" images of structures unless otherwise specified. The images were created using the Mayavi python package for all structures in order to create a benchmarked analysis.

Table of relaxation time for different NC-number

Table S3: Relaxation time for different NC-number.

Number of NCs (N)	Relaxation time (τ_R /ns)
2	11.076
4	15.967
5	21.049
6	22.386
7	27.386
8	34.417
9	34.123
10	35.601
13	41.942
15	53.083
18	58.939
21	65.639
23	70.627
25	77.189
27	80.602
28	84.384
29	85.304

Supplementary results for liquid diffusion

We show some examples in Fig. S14 of our fits where we use Eq. 13 to estimate the liquid diffusion coefficient D^l . These fits were made for $N=8,13,15,18$ and D^l values were substituted into Eq. 14 to calculate relaxation times, $T_{R,l}$. $T_{R,l}$ results are in the main paper Fig. 10b

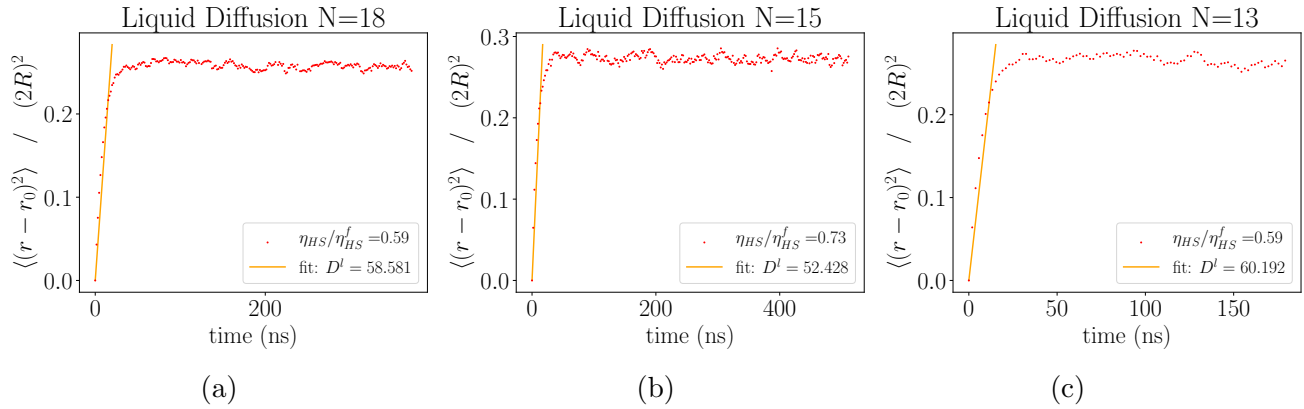


Figure S14: Diffusion coefficient, D^l , from linear fits for $N=18,15,13$.

Solvent evaporation plots used for relaxation-time estimates

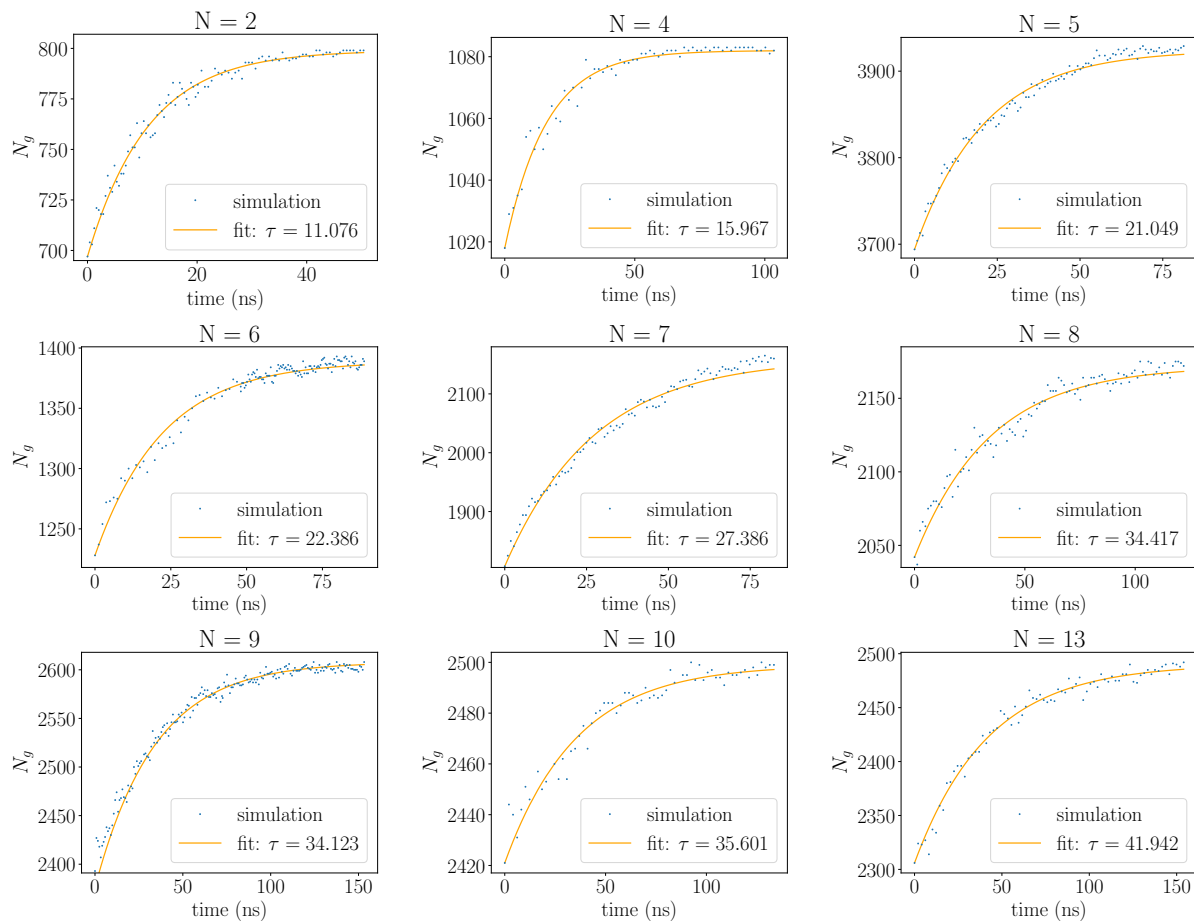


Figure S15: Number of Octane-gas particles, N_g , vs time. The blue dots are the simulation data and the orange line is Eq. 6. By fitting the simulation data we get the relaxation time, τ_R .

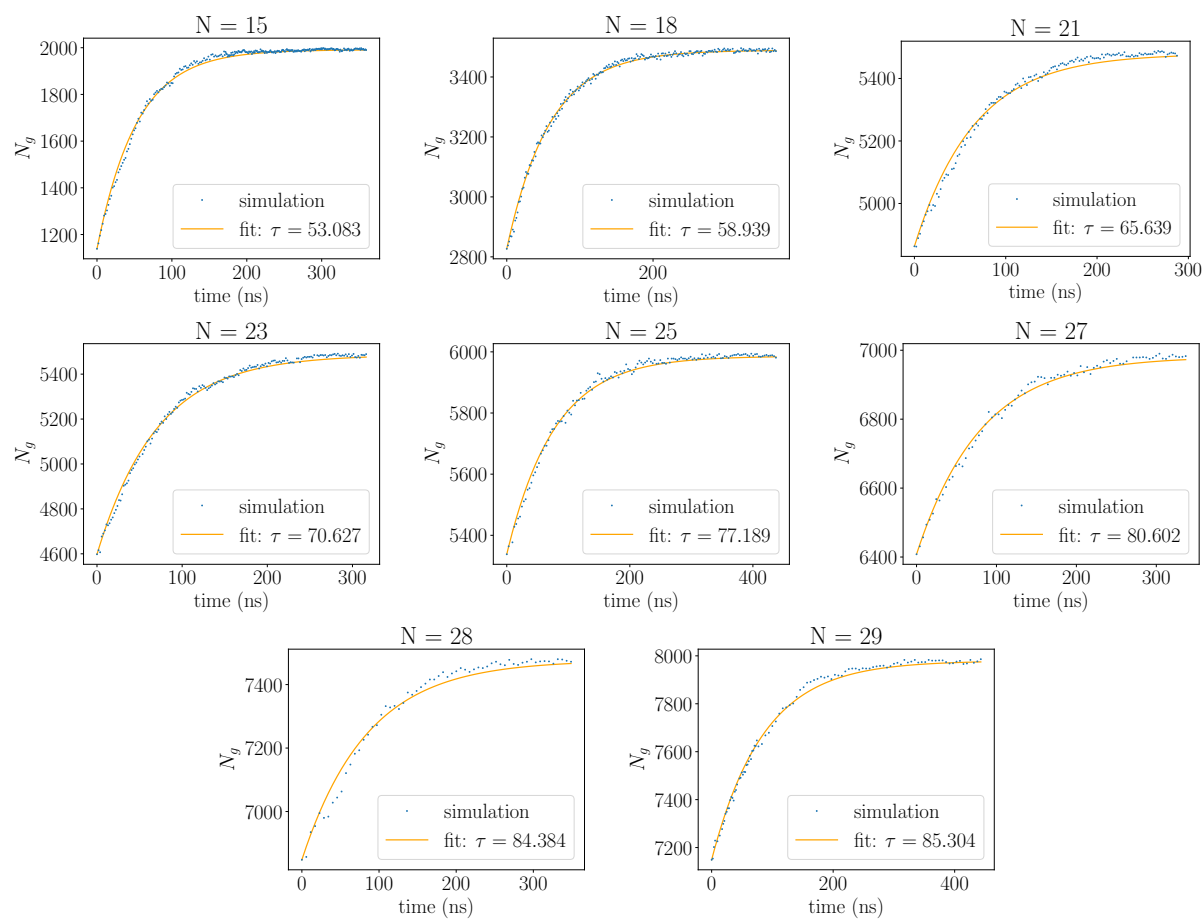


Figure S16: Number of Octane-gas particles, N_g , vs time. The blue dots are the simulation data and the orange line is Eq. 6. By fitting the simulation data we get the relaxation time, τ_R .

References

- (1) Dinpajoo, M.; Bai, P.; Allan, D. A.; Siepmann, J. I. Accurate and precise determination of critical properties from {Gibbs} ensemble {Monte} {Carlo} simulations. *The Journal of Chemical Physics* **2015**, *143*, 114113.
- (2) Smith, B. D.; Srivastava, R. *Thermodynamic data for pure compounds*; Elsevier ; Distributors for the U.S. and Canada, Elsevier Science Pub. Co.: Amsterdam; New York; New York, N.Y., U.S.A., 1986.
- (3) Allmann, R.; Hinek, R.; Rühl Stephan, A. Extended symbols of coordination polyhedra after Parthe. *Acta Cryst.* **2010**, p. 174.
- (4) Wales, D. J.; Doye, J. P. K.; A. Dullweber, M. P. H.; Calvo, F. Y. N. F.; Hernández-Rojas, J.; Middleton, T. F. The Cambridge Cluster Database. <http://www-wales.ch.cam.ac.uk/CCD.html>.